Impact of isoprene and HONO chemistry on ozone and OVOC formation in a semirural South Korean forest

[1]Saewung Kim, [2]So-Young Kim, [3]Meehye Lee, [3]Heeyoun Shim, [4,5]Glenn M. Wolfe, [6]Alex B. Guenther, and [1]Amy He, [2]Youdeog Hong, [2]Jinseok Han

1 Department of Earth System Science, School of Physical Sciences, University of California, Irvine, Irvine California, 92697 U.S.A.
2 National Institute Environmental Research, Incheon, South Korea
3 Department of Earth and Environmental Sciences, Korean University, Seoul, South Korea
4 Joint Center for Earth Systems Technology, University of Maryland Baltimore County, Baltimore, MD, USA
5 Atmospheric Chemistry and Dynamics Laboratory, NASA Goddard Space Flight Center, Greenbelt, MD, USA
6 Atmospheric Sciences and Global Change Division, Pacific Northwest National Laboratory, Richland WA USA

To be submitted to Atmospheric Chemistry and Physics “East Asian Megacity” Special Issue

Abstract

Rapid urbanization and economic development in East Asia in past decades has led to photochemical air pollution problems such as excess photochemical ozone and aerosol formation. Asian megacities such as Seoul, Tokyo, Shanghai, Gangzhou, and Beijing are surrounded by densely forested areas and recent research has consistently demonstrated the importance of biogenic volatile organic compounds (VOCs) from vegetation in determining oxidation capacity in the suburban Asian megacity regions. Uncertainties in constraining tropospheric oxidation capacity, dominated by hydroxyl radical, undermine our ability to assess regional photochemical air pollution problems. We present an observational dataset of CO, NO_X, SO_2, ozone, HONO, and VOCs (anthropogenic and biogenic) from Taehwa Research Forest (TRF) near the Seoul Metropolitan Area (SMA) in early June 2012. The data show that TRF is influenced both by aged pollution and fresh BVOC emissions. With the dataset, we diagnose HOx (OH, HO_2, and RO_2) distributions calculated using the University of Washington Chemical Box Model (UWCM v 2.1) with near-explicit VOC oxidation mechanisms from MCM 3.2 (The Master Chemical Mechanism). Uncertainty from unconstrained HONO sources and radical recycling processes highlighted in recent studies is examined using multiple model simulations with different model constraints. The results suggest that 1) different model simulation scenarios cause systematic differences in HO_X distributions especially OH levels (up to 2.5 times) and 2) radical destruction (HO_2+HO_2 or HO_2+RO_2) could be more efficient than radical recycling (RO_2+NO) especially in the afternoon. Implications of the uncertainties in radical chemistry are discussed with respect to ozone-VOC-NO_X sensitivity and VOC oxidation product formation rates. Overall, the NO_X limited regime

67 is assessed except for the morning hours (8 am to 12 pm) but the degree of sensitivity can
68 significantly vary depending on the model scenarios. The model results also suggest that
69 RO_2 levels are positively correlated with oxygenated VOCs (OVOCs) production that is
70 not routinely constrained by observations. These unconstrained OVOCs can cause higher
71 than expected OH loss rates (missing OH reactivity) and secondary organic aerosol
72 formation. The series of modeling experiments constrained by observations strongly urge
73 observational constraint of the radical pool to enable precise understanding of regional
74 photochemical pollution problems in the East Asian megacity region.

1. Introduction

NOx ($NO+NO_2$) and volatile organic compounds (VOCs) are two important precursors that drive HOx radical cycles(Levy, 1971). In the presence of NO_X, VOC oxidation processes recycle OH and produce photochemical oxidation products such as ozone and oxygenated VOCs (OVOCs). This reaction cycle is highly non-linear. For example, excess NO_2 may expedite nitric acid formation (R1), limiting ozone production. In the same context, excess VOCs may expedite peroxy radical production (R2), which limits OH regeneration from peroxy radicals.

$$OH + NO_2 + M \rightarrow HNO_3 + M \quad (R1)$$

$$HO_2 + RO_2 \rightarrow ROOH \quad (R2)$$

The non-linearity in tropospheric photochemistry has been relatively well studied in the urban regions of developed countries and applied in ozone reduction policy. The Los Angeles Metropolitan Area has accomplished significant ozone reduction by implementing aggressive emission reductions of both NOx and VOC especially from mobile sources (Ryerson et al., 2013). The remarkable ozone abatement was possible due to the fact that there is no significant pollution transport from other metropolitan areas and no significant natural emission sources especially volatile organic compounds from vegetation (BVOCs; biogenic volatile organic compounds) compared with anthropogenic VOC mostly from mobile sources (Pollack et al., 2013;Huang et al., 2013). In the late 80s, Trainer et al. (1987) first demonstrated the importance of isoprene (C_5H_8) as a peroxy radical source that can contribute significant ozone production in rural areas. The

98 importance of isoprene in ozone production in urban areas has also been highlighted, e.g.
99 in the Atlanta Metropolitan Area (Chameides et al., 1988).
100 Isoprene is a hemiterpenoid species and is the globally dominant VOC emission
101 from vegetation (Arneth et al., 2011;Guenther, 2013). Arguably, isoprene is the most
102 frequently studied BVOC from the perspective of atmospheric oxidation processes and
103 their implications for ozone and aerosol formation. However, significant uncertainty
104 hinders assessing the roles of isoprene in regional and global photochemistry in three
105 fronts. First, there is still significant uncertainty in estimating emission rates from each
106 individual plant species on regional scales (Guenther, 2013). Second, limited isoprene
107 inter-comparison results (Barket et al., 2001) suggest that there are large systematic
108 biases among different analytical techniques. Lastly, recent laboratory, theoretical and
109 field observations suggest significant uncertainty in tropospheric isoprene oxidation
110 processes initiated by OH. Until early 2000, it was thought that three first generation
111 isoprene oxidation products (methyl vinyl ketone, methacrolein, and formaldehyde) from
112 OH oxidation were enough to constrain isoprene tropospheric oxidation processes for
113 modeling purposes (e.g. Spaulding et al. (2003) and Dreyfus et al. (2002)). This is an
114 interesting evolution of thoughts considering that Paulson and Seinfeld (1992), one of
115 pioneering works describing isoprene oxidation, clearly claimed that 22 % of first
116 generation isoprene oxidation products from the reaction with OH was not identified and
117 likely included multifunctional C5 compounds. Recent advances in analytical techniques
118 (Kim et al., 2013a) have shown that indeed significant C5-hydroxy carbonyl (e.g.
119 isoprene hydroperxyenals, HPALD) and peroxide compounds are produced as first
120 generation isoprene oxidation products (Crounse et al., 2011;Paulot et al., 2009;Wolfe et

al., 2012;Zhao and Zhang, 2004). The product yields appeared to be a strong function of NO concentrations (Peeters and Muller, 2010). In general, at low to intermediate NO levels (~ 100 pptv or lower), the yields of C5-hydroxy carbonyl compounds become higher. These new findings in the isoprene oxidation process are also closely related with recent findings in unexpectedly high OH concentrations (Hofzumahaus et al., 2009;Lelieveld et al., 2008) and substantial missing OH sinks also known as unexpectedly high OH reactivity in high isoprene environments (Di Carlo et al., 2004;Edwards et al., 2013;Kim et al., 2011;Lou et al., 2010).

These new findings have significant implications for regional air quality especially regarding photochemical ozone and SOA production. Despite the strong anthropogenic pollutant emissions in East Asia (China, Japan and South Korea), recent research has shown that isoprene accounts for a major OH chemical sink in suburban areas near Beijing (Ran et al., 2011), the Pearl River Delta region (Lu et al., 2012), Taipei (Chang et al., 2014) and Seoul (Kim et al., 2013d;Kim et al., 2013b). Consequently, modeling studies also clearly show that isoprene contributes significantly to ozone formation in Asian megacity regions. Kim et al. (2013d) reported that simulated ozone levels with isoprene chemistry are up to 30 % higher than ozone simulation without isoprene chemistry using the WRF-Chem model, indicating an urgent need to implement improved isoprene chemistry schemes in these models in order to simulate the unexpected higher levels of OH in isoprene rich environments. This could become an especially serious issue as Hofzumahaus et al. (2009) reported significantly higher (~ 2.6 times at noon) than expected OH levels in the Pearl River Delta region in China. Therefore, the current assessments based on the conventional OH photochemistry could

144 significantly misdiagnose regional air-quality status and mislead policy implementation
145 to reduce photochemical air pollution in the East Asian region. Furthermore, as the
146 importance of BVOC in regional air-quality issues in ozone and SOA formation has been
147 also highlighted in Europe and North America, the uncertainty in isoprene
148 photochemistry has significant implications in urban and suburban air quality in general
149 (Zhang et al., 2008a;Sartelet et al., 2012). It should be also noted that HONO has been
150 observed in high-levels in the East Asian region even in the daytime (~ hundreds ppt,
151 (Song et al., 2009;Hao et al., 2006;Li et al., 2012)). The data analysis has consistently
152 indicated that well-known HONO sources cannot account the observed level. Therefore,
153 the implications of HONO as a radical source should also be comprehensively addressed.
154 We present atmospheric observations of NO_X, CO, VOCs, ozone, and HONO in
155 the Taehwa Research Forest (TRF) in the Seoul Metropolitan Area (SMA), South Korea.
156 We use observed data from June, 2013 to conduct observationally constrained box model
157 (University of Washington Chemical Box Model; UWCM) calculations to estimate OH,
158 HO_2 and RO_2 concentrations with different sets of observational parameters. We discuss
159 current uncertainty in OH-isoprene photochemistry with perspectives of constraining
160 photochemical ozone production and OVOCs precursors of secondary organic aerosols in
161 addition to the roles of unconstrained HONO sources in radical distributions.
162
163 2. **Methods**
164 The Taehwa Research Forest (TRF) is located ~ 35 km from the center of Seoul,
165 South Korea. The TRF is located at the southeastern edge of the Seoul metropolitan Area
166 (SMA, population of ~ 23 million). TRF has a sampling tower located in the middle of a

167 coniferous tree plantation (200 m by 200 m) with the canopy height of 18 m (*Pinus*
168 *koraiensis*) surrounded by a deciduous forest mostly composed by oak. The TRF
169 instrumentation has previously been described by Kim et al. (2013d) along with the
170 previous trace gas observational results. Therefore, just brief descriptions of analytical
171 techniques are given in this paper.
172
173 **2.1. CO, NO_X, SO_2, ozone, VOCs, and meteorological parameters**
174 Thermo Fisher Scientific Enhanced Trace Level Gas Analyzers are used for CO,
175 NO_X, SO_2, and ozone observations as summarized Table 1. A molybdenum (Mo)
176 converter is used to convert NO_2 to NO for the NO_X analyzer. Although Mo converters
177 are still widely used for NO_2 observations, some of thermally unstable oxygenated
178 reactive nitrogen compounds, especially peroxyacyl nitrates, could be also converted to
179 NO_2 by a Mo-converter (Villena et al., 2012). VOC observations are conducted by a
180 High-Sensitivity Proton Transfer RPANeaction-Mass Spectrometer (PTR-MS, Ionicon
181 GmbH). The atmospheric application of this technique is thoroughly reviewed by de
182 Gouw and Warneke (2007). In addition, the instrument suite at TRF is thoroughly
183 described in (Kim et al., 2013d). PTR-MS can quantify atmospheric VOCs that have
184 higher proton affinity than the proton affinity of H_2O (691 kJ mol^{-1}). Most alkanes have
185 lower proton affinity than water but alkene, aromatic and some OVOCs have higher
186 proton affinity and are suitable for quantification using PTR-MS (Blake et al., 2009).
187 These compounds are more reactive than alkane compounds so PTR-MS has capability to
188 observe reactive atmospheric compounds. The TRF PTR-MS system was set to measure
189 acetaldehyde, acetone, acetic acid, isoprene, methylvinylketone (MVK) + methacrolein

(MACR), MEK, benzene, xylene (*p*, *m*, and *o*), and monoterpenes (MT). Each compound was set to be monitored for 1 second each resulting in a sample cycle of 15 seconds. Lower detection limits for the observed VOCs are estimated to be 20 ppt for a 5 second integration with sensitivity of 70 counts ppb^{-1} (2 σ). The uncertainty is estimated as 12 % (2 σ) for the same integration time. Meteorological parameters such as temperature and humidity are monitored by LSI LASTEM Meteorological Sensors. All the presented data is from the 15 m (the canopy height is 18 m) sampling line and meteorological sensors collocated at this height too.

PTR-MS with a quadrupole mass filter has an intrinsic limitation that isobaric compounds are all collectively quantified with the same channel (m/z) with a resolution of unit mass. This limitation particularly becomes an issue for investigating the roles of different isomers of MT and sesquiterpenes (SQTs) in photochemistry. For this reason, we also occasionally collect sorbent cartridge samples to analyze MT and SQT speciation in both ambient air and branch enclosure emissions near the sampling tower. As described in (Kim et al., 2013d), Tenax GR and Carbotrap 5TD packed sorbent cartridges (Markes Int, Llanstrisant, UK) were used for sampling. The sampled cartridges were shipped to National Center for Atmospheric Research (NCAR), Boulder CO, USA for gas chromatography-mass spectrometer (GC-MS) analysis. An Agilent 7890 GC/5975 C Electron Impact Mass Spectrometer (GC-MS/FID) in conjunction with a MARKES Unity1/Ultra thermal desorption system optimized for terpenoid analysis quantifies speciated MT and SQT in the sorbent samples. Cartridge samples are both collected from ambient and branch enclosure air. Ambient samples were collected in the mid-day to early afternoon with a volume of 6 L. Ozone in the ambient air was removed using a

213 Na_2SO_3 filter. Branch enclosure samples were also collected, mostly in the mid-day time
214 frame, with a volume of 1 L without an ozone filter as zero air was introduced to the
215 branch enclosure. To explore the diurnal differences in BVOC emissions, branch
216 enclosure samplings were conducted every two hours for three consecutive days in mid
217 June of 2013. We present these analytical results from GC-MS analysis limited to the
218 qualification purpose to examine MT and SQT speciation.
219
220 **2.2 HONO quantification**
221 HONO was measured with an ion chromatography (IC) coupled with diffusion
222 scrubber. Air was introduced to diffusion scrubber (Lab solutions Inc., IL, USA) through
223 a 2 m PFA tubing (1/4" i.d.) at 1.5 L m^{-1} using a filtered orifice restrictor (F-950, air
224 logic, WI, USA). Air flowing through diffusion scrubber interfaced with deionized water,
225 into which HONO was extracted. 50 μL of solution was injected into the IC system
226 through a PEEK loop (Rheodyne, WA, USA) and 6-way valve (EV750-100, Rheodyne,
227 WA, USA). Eluent was a mixture of Na_2CO_3 and $NaHCO_3$, which was pumped by a
228 HPLC pump (DX-100, Dionex, CA, USA) into a guard column (Ionpax® AG 14,
229 4x50mm, Dionex, CA, USA) and then analytical column (Ionpax® AS 14, 4x250mm,
230 Dionex, CA, USA). The column effluent passed through a suppressor (ASRS 300,
231 Dionex, CA, USA) and HONO was detected as nitrite ion in conductivity detector (550,
232 Alltech, IL, USA). The entire measurement processes of sampling, chemical analysis, and
233 data acquisition were controlled by a digital timer and data acquisition software
234 (DSchrom-n, DS science, Korea), by which we obtained two measurements every hour.
235 The system was calibrated using a NO_2^- standard solution (Kanto chemical Co., Inc.,

236 Tokyo, Japan) whenever reagents were replaced. The detection limit was 0.15 ppb
237 estimated from 3σ of the lowest working standard. Specific analytical characteristics are
238 described in Simon and Dasgupta (1995) and Takeuchi et al. (2004).
239
240 **2.3 UWCM box model**
241 UWCM 2.1 is an open source box model coded by MATLAB (MathWorks®).
242 The model platform can be downloaded from a website
243 (http://sites.google.com/site/wolfegm/code-archive). The box model is embedded its own
244 HO_X ($OH+RO_2$)-RO_X (peroxyradical and alkoxy radical)-NO_X coupling chemical
245 mechanism. UWCM utilizes Master Chemical Mechanism version 3.2 (MCM 3.2)
246 (Jenkins et al., 1997; Saunders et al., 2003) for near-explicit VOC photo-oxidation
247 schemes. A more detailed model description can be found in Wolfe and Thornton (2011).
248 To minimize uncertainty from the parameterizations of transport and emission, we
249 constrained relatively long-lived trace gases presented in Figure 1. This box modeling
250 technique has been commonly used for examination of OH levels that can be justified by
251 the short chemical lifetime of OH (Kim et al., 2014;Kim et al., 2013c;Mao et al.,
252 2012;Mao et al., 2010). Recently developed isoprene photo-oxidation mechanisms
253 shown in Archibald et al. (2010b) are also incorporated in the model. In addition, Kim et
254 al. (2013c) and Wolfe et al. (2013) applied the model in the identical fashion as used for
255 this study to probe radical distributions using comprehensive observational datasets. This
256 study used the UWCM to simulate the diurnal variations of radical pool ($OH+HO_2+RO_2$)
257 distributions as observational parameters such as CO, NO_X, ozone, and VOCs are
258 constrained. To fully account for roles of OVOCs in the box model as radical sources, we

simulated three consecutive days and presented diurnal variations from the third day. The specific parameters (CO, NO_X, ozone, HONO and VOCs), constrained by observations are described in section 2.1 and 2.2 and presented in Figure 1.

3. Results and Discussion

3.1. Observational Results

Diurnal averages of observed trace gases (June 1st 2013 to June 6th 2013) are shown in Figure 1. The TRF observatory is in continuous operation and we choose this six day period because a regional high-pressure system caused a stagnant air pollution event in this period. In the center of Seoul (the real-time data available at http://www.airkorea.or.kr), carbon monoxide was observed in the similar levels during the focused period (June 1st to June 6th, 2013). On the other hand, the NO_2 level observed in central Seoul was much higher (20-50 ppb) compared with observed levels at TRF. The reason can be attributed to differences between the chemical lifetime of CO (~a month) and NO_2 (~a few hours to a day). The observations clearly indicate that the TRF is not directly influenced by fresh SMA pollution plumes although the TRF is very close to the center of Seoul (30 km away from the city center) as a regional modeling study shows most of CO and NO_X sources are located in the city center (Ryu et al., 2013). Similar observations were also reported for other East Asian megacities such as Beijing (Ma et al., 2012), where ~ 30 ppb and ~ 15 ppb of NO_2 were observed at noon in the urban and the adjacent rural sites, respectively. In contrast, there were no noticeable differences in CO levels between the urban and rural sites (~ 1-2 ppm). The observed CO, NO_X and SO_2 levels in TRF were much lower than those observed in the suburban

282 regions of Chinese megacities such as Beijing (Ma et al., 2012), Shanghai (Tie et al.,
283 2013), and the Pearl River Delta Region (Lu et al., 2012) and similar with the observed
284 levels in Tokyo, Japan (Yoshino et al., 2012).

285 Previous VOC observations in the SMA consistently have shown that toluene is
286 the dominant anthropogenic VOC followed by other aromatic compounds such as xylene
287 and benzene (Kim et al., 2012;Na and Kim, 2001). Na and Kim (2001) reported high
288 concentrations of propane from house hold fuel use. However, recent observation results
289 from the photochemical pollution observational network managed by National Institute of
290 Environmental Research (NIER) of South Korea in the SMA clearly indicate that propane
291 levels have declined and are now much lower than the levels previously observed (NIER,
292 2010). This is probably caused by the implementation of a policy changing household
293 fuel sources from propane to methane. Kim et al. (2012) presented detailed aromatic
294 VOC distributions in the SMA from four different urban observational sites. In average,
295 toluene concentrations were observed ~ 7 times higher than the observed levels of xylene
296 and benzene. At the TRF, a similar anthropogenic VOC speciation distribution was
297 observed as shown in Figure 1. The observed toluene and MEK (methyl ethyl ketone)
298 mixing-ratios were much higher than benzene and xylene. MEK is detected in m/z of 73^+
299 by PTR-MS. Although methyl glyoxal, an atmospheric VOC oxidation product, is also
300 detected on the same mass, we assumed that 73^+ of m/z signals are mostly from MEK, an
301 anthropogenic VOC, since the temporal variation follows that of anthropogenic VOC
302 such as toluene and xylene. In addition, atmospheric lifetime of methyl glyoxal is much
303 shorter than MEK.

As the observation facility is located in the middle of a pine tree plantation (*Pinus koraiensis*), monoterpenes (MT) are consistently observed. The temporal variation of monoterpenes is affected by the planetary boundary layer evolution with a pattern of higher MT levels during night than those of mid-day as has been often reported in other forest environments (Bryan et al., 2012;Kim et al., 2010) This can be explained by interplays between boundary layer evolution and temperature dependent MT emission. It should also be noted that the continuous branch enclosure BVOC emission observations indicate that the daily maxima of MT and SQT emissions were observed in the midday (between noon to 2 pm in the local time). The observed MT and SQT speciation information in the midday is summarized in Table 2. Table 2a summarizes branch enclosure sample analysis results and ambient sample analysis results are summarized in Table 2b. In general, observed MT and SQT in the ambient air are consistent with previously observed distributions (Kim et al., 2013d). α-pinene and β-pinene were the dominant monoterpene and longifolene was the only detected SQT species. In contrast, the branch enclosure observation results, reflecting BVOC emission, indicate high emission of very reactive MT and SQT species such as β-myrcene, α-caryophyllene, and β-caryophyllene. The fast oxidation of these highly reactive terpenoid species is expected to limit the atmospheric presence of the compounds. Therefore, photochemical oxidation processes of these compounds may have been neglected. Investigating emissions and photochemistry of these reactive terpenoid compounds can constrain potential missing OH reactivity and SOA production from highly oxidized reaction products.

Isoprene is produced from carbon recently fixed through photosynthesis resulting in higher emissions and atmospheric concentrations during the daytime. The temporal

variation shown in Figure 1 reveals an isoprene concentration maximum between 17:00 to 20:00. In addition, the ratios of MVK+MACR, major isoprene oxidation products and isoprene at this period, are significantly lower than those of late morning to early afternoon. The enhanced isoprene levels in the late afternoon or early evening have been also reported in previous studies (Apel et al., 2002;Bryan et al., 2012). The branch enclosure observations demonstrate that isoprene is not emitted from the pine plantation but rather transported from surrounding broadleaf forests as right outside of the pine plantation (200 m × 200 m) is a forested area dominated by oak trees. Oak comprises 85 % of broadleaf trees in South Korea (Lim et al., 2011). Lim et al. (2011) quantified isoprene emission rates for five representative oak species in South Korea and report a wide emission range from oaks that are negligible isoprene emitters (<0.004 μgC dw^{-1} h^{-1}; standard emission rates) to others with very high isoprene emission rates of 130 μgC dw^{-1} h^{-1}. It is also noticeable that isoprene is observed in high levels (up to 1 ppb) even during the night. Observational results from the Pearl River Delta region in China also show high isoprene concentration episodes of more than 1 ppb during the night (Lu et al., 2012). As there are some speculations on potential artifacts on isoprene measurements using PTR-MS in environments with large oil and gas evaporative sources (Yuan et al., 2014), the assessments of the potential artifacts should be investigated further in the Asian megacity region.

Contributions from each trace gas species towards ambient OH reactivity are shown in Figure 2. This is calculated as the product of the observed species concentration and its rate constant for reaction with OH. Observed OH reactivity from VOCs are much higher than from other trace gases such as CO, NOx, SO_2, and ozone. Among the

observed VOC species, BVOCs such as isoprene, α-pinene and β-pinene accounted for significantly higher OH reactivity in comparison with the observed AVOCs such as toluene, benzene, xylene and MEK. Isoprene accounts the highest OH reactivity especially during the daytime. This analysis is consistent with reports from other suburban observations from East Asian megacities such as Beijing (Ran et al., 2011), the PRD region, China (Lou et al., 2010), and the Kinki region Japan (Bao et al., 2010).

HONO levels up to 1 ppb were observed in the early morning and were consistently higher than 0.5 ppb during the daytime. These observed levels are substantially higher than reported observations from forest environments in North America (Ren et al., 2011;Zhou et al., 2011), where NO_X (~ 1 ppb) is substantially lower than the level observed at TRF. Ren et al. (2011) reported 30 – 60 ppt of HONO at the Blodgett Forest Research Station in the western foothills of the Sierra Nevada Mountains in the late summer of 2007. Zhou et al. (2011) also reported the similar levels of HONO (below 100 ppt) from the PROPHET forest, a mixed hardwood forest in northern Michigan (Pellston, MI). However, significantly higher HONO levels (~ 200 ppt to ~ 2 ppb) were reported by Li et al. (2012) from a rural observational site in the Pearl River Delta region near Guangzhou, where comparable NO_2 levels with TRF were observed. The high HONO levels (a few hundred ppt) especially during the daytime have been consistently reported near Eastern Asian megacities such as Beijing (Li et al., 2012), Shanghai (Hao et al., 2006), and Seoul (Song et al., 2009). Still these are limited datasets and further comprehensive analysis, especially more extensive observation is required. However, recently proposed HONO production mechanisms may be able to explain the higher levels in the Eastern Asian megacity region. One is HONO production from NO_2

373 photo-excitation (Wong et al., 2012) as the region usually has high NO_2 concentrations.
374 Zhou et al. (2011) claimed that significant HONO could be generated from nitrate
375 photolysis processes on forest canopy surface by presenting observational data from a
376 hardwood forest in Pellston, MI. Finally, HONO emission from soil bacteria is also
377 proposed (Oswald et al., 2013). Oswald et al. (2013) found differences as much as two
378 orders of magnitude in HONO emissions from soil samples from different environments
379 (e.g. pH and nutrient contents). In addition, as most of observations in the East Asia
380 regions were conducted with ion chromatography based methods, more direct HONO
381 quantification techniques such as a chemical ionization mass spectrometry technique
382 (Roberts et al., 2010) need to be used to characterize any potential interferences such a
383 high NO_X environment (e.g. N_2O_5).
384
385 **3.2 HO_X Model calculations to examine different isoprene photo-oxidation scenarios**
386 **and the roles of unconstrained HONO sources.**
387 The presented observational results are used to constrain the UWCM box model.
388 We evaluate uncertainties in the tropospheric oxidation capacity and how it affects our
389 ability to constrain ozone and OVOCs production. The observational results clearly
390 indicate that isoprene is the most dominant OH sink among the observed VOCs. In
391 addition, NO concentrations were higher in the 600 to 800 ppt range in the morning. On
392 the other hand, afternoon levels were substantially lower in the 50 to 100 ppt range. The
393 environment provides a unique opportunity to examine implications of isoprene
394 photochemistry in various NO conditions.

We conducted model simulation under four different scenarios. Each scenario is described in Table 3. The quantitative assessments of the impacts on radical concentrations (OH, HO_2, and RO_2) from unknown HONO sources are evaluated by examining the outcomes of the model simulations with and without observed HONO. To evaluate the impacts of hydroperoxy-methyl-butenal (HPALD) photolysis and isoprene peroxy radical recycling in the radical pool, each chemical mechanism is selectively constrained by different scenarios. For HPALD chemistry, we adapted two different HPALD formation rate constants published by Peeters and Muller (2010) and Crounse et al. (2011). The formation rates from Peeters and Muller (2010) are about 40 times faster than those from Crounse et al. (2011) in 298 K. Although there have been speculations about other radical recycling mechanisms such as peroxy radical-peroxy radical reactions (Lelieveld et al., 2008) and unknown reducing agents showing similar chemical behaviors as NO (Hofzumahaus et al., 2009), we do not evaluate these possibilities as there are no specific chemical mechanisms.

Modeled OH, HO_2, and RO_2 from the four different model scenarios are shown in Figure 3. A summary of averaged OH, HO_2, and RO_2 concentrations in the morning (08:00 – 11:00) and the afternoon (13:00 – 16:00) from each simulation is shown in Table 4. With respect to the base run results (Scenario I), Scenario III with the lower HPALD formation rate does not cause noticeable differences in radical concentrations. Adapting higher HPALD formation rates (Scenario II) cause significant differences in radical distribution especially in RO_2. This difference is likely caused by the fact that significant isoprene peroxy radical is converted to HPALD. The higher levels of discrepancy is found in RO_2 between Scenario I and Scenario II in the afternoon when

418 low NO concentrations are observed, which efficiently facilitates HPALD formation.
419 Similarly, a larger OH discrepancy (~ 20 %) between Scenario I and Scenario II is
420 observed in the afternoon.

421 Striking differences can be found in the model simulation results with or without
422 constraining observed HONO as shown in Figure 3. Model calculation results from
423 Scenario IV indicate significantly smaller OH, HO_2, and RO_2 concentrations than the
424 concentrations calculated from the counter part (Scenario I), which contains identical
425 constraints and isoprene photochemistry except constraining observed HONO. Again,
426 this clearly indicates that more thorough evaluations of the impacts of HONO on air
427 quality are needed to precisely constrain photochemical processes in the region along
428 with evaluations of the currently available analytical techniques as argued in section 3.1.
429

430 **3.3 Implications of the uncertainty in HO_X estimations in assessing photochemical**
431 **ozone and OVOC production.**

432 Two competing chemical reactions (R3 vs. R4,5,6) determine radical distribution
433 regimes.

434 $$RO_2 + NO \rightarrow RO + NO_2 \quad (R3)$$

435 $$RO_2 + HO_2 \rightarrow ROOH + O_2 \quad (R4)$$

436 $$RO_2 + RO_2 \rightarrow ROOR + O_2 \quad (R5)$$

437 $$HO_2 + HO_2 \rightarrow H_2O_2 + O_2 \quad (R6)$$

438

439 When the rate of R3 gets much faster than the sum of reaction rates of R4, R5,
440 and R6 then radical recycling processes become more efficient than radical destruction

441 processes. In this radical recycling regime, OH, a universal tropospheric oxidant, is well
442 buffered to maintain the elevated OH levels. On the other hand, the radical destruction
443 regime can be defined when the radical recycling rates (R3) are slower than the radical
444 destruction reaction rates (R4+R5+R6). Although some recent field studies (e.g.
445 Lelieveld et al. (2008)) suggest that we may need to reconsider R4 as a radical recycling
446 process rather than a radical destruction process, in this study, we follow the conventional
447 classification of radical chemistry regimes since recent laboratory characterizations have
448 shown that OH recycling from the RO_2+HO_2 reaction should be insignificant (Liu et al.,
449 2013;Villena et al., 2012;Fuchs et al., 2013) . The temporal variations of radical-radical
450 reaction rates from the model simulation scenarios are shown in Figure 4. In general, the
451 radical reaction rates are elevated as much as twice once observed HONO is constrained
452 in the model calculations (e.g. Scenario IV). This is because unaccounted HONO in the
453 model calculations cause significant underestimations in the radical pool ($OH+HO_2+RO_2$)
454 size with respect to the constrained HONO scenarios as shown in Figure 4. In addition, in
455 the afternoon when NO concentration becomes lower, the RO_2 + HO_2 reaction rates get
456 close or slightly higher than those of RO_2 + NO in the afternoon for the all model
457 scenarios, constrained by observed HONO. This is surprising, as the radical destruction
458 regime is usually associated with low NO_X conditions. Suburban regions of megacities
459 including the TRF in general show high NO_X conditions. However, radical recycling
460 rates are determined by concentrations of NO. The fraction of NO in the NO_X pool is
461 determined by competing reactions between NO_2 photolysis and oxidation reactions of
462 NO by ozone, HO_2, and RO_2 radicals. Once we assume the pseudo-steady state of NO,
463 then NO in NO_X pool (Leighton, 1961) can be expressed as

$$[NO] = J_{NO2}[NO_2]/(k_{NO+O3}[O_3] + k_{NO+HO2}[HO_2] + k_{NO+RO2}[RO_2]) \quad \text{(Eq 1)}$$

This mathematical expression clearly shows that NO levels are dependent on NO_X mostly composed of NO_2. At the same time, the fraction of NO in NO_X is anti-correlated with ozone, HO_2, and RO_2 concentrations. Therefore, the size of the radical pool composed of HO_2 and RO_2 is relevant for determining the fractions of NO in given NO_X levels. High HO_2 and RO_2 are likely observed in high VOC regions such as forested areas. This could cause a smaller fraction of NO in the given NO_X pool so radical recycling gets relatively weaker compared with radical destruction reaction pathways. More quantitative approaches are required to categorize radical reaction pathways rather than qualitative categorization such as high or low NO_X regimes. One should keep in mind that the pseudo-steady state assumption requires precise NO_2 quantification, which may not be the case in our study as the Mo-converter used for the NO_2 quantification could have interferences (Table 1). The overestimation due to thermal dissociations of reactive oxygenated nitrogen species has been reported to be 20 % to 83 % (Ge et al., 2013;Steinbacher et al., 2007). In addition, Mannschreck et al. (2004) presented the NO-NO_2-ozone photostationary state analysis using a four year dataset from a rural observational site in Hohenpeissenberg, Germany. The results indicate that the pseudo steady state assumption considering only NO-NO_2-ozone deviates about a factor of two from the stationary state on average. Even with the consideration of peroxy radical chemistry the pseudo steady state assumption is only valid for 13-32 % of the observational period. The authors speculated that local NO_2 sources, local NO or ozone

487 sinks, or rapid changes in J_{NO2} and ozone can break the pseudo-steady state. Nonetheless,
488 the argument that NO is a more critical parameter in determining radical distributions
489 than NO_X levels still holds.
490 Conventionally, efficient ozone production can be achieved by the balance
491 between nitric acid production rates (P_{HNO3}, OH + NO_2) and peroxide production rates
492 (P_{ROOH}, HO_2+RO_2 or P_{H2O2} HO_2+HO_2) (Sillman and He, 2002). The imbalance will cause
493 ozone production sensitivity towards either NOx or VOCs. A comprehensive
494 photochemical model analysis (Tonnesen and Dennis, 2000a, b) demonstrated that in a
495 wider range of ozone concentrations, the VOC and NOx limited regimes can be
496 determined by the ratios of P_{H2O2} and P_{HNO3}. Kleinman (2000) and Sillman and He (2002)
497 presented an observation-based ozone production regime evaluation method comparing
498 peroxide production rates (P(peroxide)) and nitric acid production rates ($P(HNO_3)$). This
499 categorization has guided policy-making processes whether NO_X or VOC controls will be
500 more effective in ozone reduction. A series of modeling studies have been conducted to
501 characterize ozone production regimes in the suburban regions of East Asian megacities
502 and have consistently concluded that the role of isoprene is important in ozone
503 production. However, most of these studies have concluded that East Asian megacity
504 regions are mostly in the VOC limited regime (Tseng et al., 2009;Zhang et al.,
505 2008b;Lim et al., 2011;Cheng et al., 2010;Shao et al., 2009a;Shao et al., 2009b;Xing et
506 al., 2011). Recently, however, a modeling study by Li et al. (2013) in the Pearl River
507 Delta region in China demonstrated the time dependence of ozone production regimes.
508 Specifically, with high NOx emissions in the morning, the regional ozone production
509 regime is categorized as VOC limited. In contrast, in the afternoon when the highest

510 ozone concentrations are observed, a NOx limited regime is often found. In addition, a
511 box modeling study constrained by observation on top of Mt. Tai in Central East China
512 also reported NO_X limited ozone production regime (Kanaya et al., 2009). The obvious
513 issue to be addressed is that all of the above studies neglected how the uncertainty in
514 hydroxyl radical chemistry would affect the ozone production regime. Moreover, HONO
515 has been rarely constrained by observations in the previous modeling studies. Figure 5
516 shows the temporal variations of 2 P(peroxide)/P(HNO_3) from all four different model
517 scenarios. As shown in the figure, the ratio above 1 indicates the NO_X limited regime and
518 the VOC limited regime can be determined when the ratio is below 1. The NO_X limited
519 ozone formation regime occurred on most days except the morning when high NO_X
520 levels were observed regardless of the HO_X simulation scenarios. This is consistent with
521 the recent modeling study for the Pearl River Delta region by Li et al. (2013). Differences
522 among the scenarios are not noticeable in the morning when NO is high but noticeable
523 differences can be found in the afternoon which may cause uncertainty in assessing the
524 optimal level of NO_X and VOC emission controls from a policy perspective. In general,
525 the model calculation results with faster HPALD formation rates indicate lower
526 2P(peroxide)/P(HNO_3) in the afternoon. This analysis indicates that it is difficult to
527 determine an effective policy implementation for NO_X or VOC controls to achieve ozone
528 abatement around Asian megaticities where isoprene is a significant OH sink without
529 accurate understanding of radical-isoprene interactions (e.g. Kim et al. (2013b)). Again, it
530 should be noted the possibility of systematic NO_2 overestimations from the Mo-converter
531 use as discussed. The overestimation will directly translate into overestimated P(HNO_3).

532 Therefore, it is likely that the ozone production regime at TRF is shifted towards the NO_X
533 limited regime in reality.
534 Another unresolved uncertainty in understanding tropospheric OH is its chemical
535 loss rates. The limited observations of OH reactivity in BVOC dominant environments
536 show consistent unaccounted OH chemical loss with observational datasets (Di Carlo et
537 al., 2004;Edwards et al., 2013;Kim et al., 2011;Lou et al., 2010;Nolscher et al.,
538 2012;Nakashima et al., 2014;Sinha et al., 2010). Two different processes are speculated
539 to cause unaccounted OH loss known as missing OH reactivity: 1) primary emissions of
540 unmeasured or unknown compounds and 2) oxidation products of well-known BVOCs
541 especially isoprene. Most studies conducted in coniferous forests where monoterpenes
542 are dominant primary BVOC emissions have concluded that unmeasured or unknown
543 primary BVOC emissions caused missing OH reactivity (Sinha et al., 2010;Nakashima et
544 al., 2014). On the other hand, studies conducted in isoprene dominant environments in
545 mostly broadleaf or mixed forests have concluded that the main cause of missing OH
546 reactivity is the oxidation products of isoprene (Edwards et al., 2013;Kim et al., 2011).
547 Edwards et al. (2013) presented a thorough analysis on potential impacts of isoprene
548 oxidation products that are not routinely constrained by observations. The authors found
549 significant contributions from secondary oxidation products such as multi-functional
550 oxygenated compounds.
551 Figure 6a shows the temporal variations of total OH reactivity calculated from
552 five different model scenarios (I through IV). The highest and the lowest OH reactivity
553 levels were predicted from model calculations of Scenario I and Scenario IV, respectively.
554 This observation is directly correlated with calculated RO_2 levels as the lowest and

555 highest RO_2 levels were calculated from Scenario I and Scenario IV, respectively. Since
556 VOC precursors and trace gases were all constrained by observations in the model
557 calculations, the differences in model calculated OH reactivity should be mainly caused
558 by the oxidation products of VOCs. This can be confirmed by the comparisons of model
559 calculated formaldehyde concentrations from Scenario I and IV as formaldehyde is a
560 dominant oxidation product of isoprene (Figure 6b). The differences in formaldehyde
561 levels suggest differences in OH reactivity levels from OVOCs in each model simulation.
562 In summary, uncertainty in radical distributions especially RO_2 levels is directly
563 propagated into uncertainty in OVOC formation.

564 These calculated results provide an upper limit of potential contributions from the
565 oxidation products of the constrained VOC precursors considering that the box-model
566 does not consider dry-deposition processes as Karl et al. (2010) and Edwards et al. (2013)
567 suggested that there is significant uncertainty associated with the parameterizations of dry
568 deposition especially OVOCs. Still, this analysis suggests that significant missing OH
569 reactivity can be found without constraining OVOCs. OVOCs, especially multi-
570 functional highly oxidized compounds are precursors for secondary organic aerosols
571 (SOA). Therefore, uncertainty surrounding missing OH reactivity significantly
572 undermines our ability to constrain SOA formation and aerosol growth.

573

574 ## 4. Summary and conclusions

575 We presented trace gas observation results from the TRF near the center of Seoul,
576 South Korea. The dataset provides important constraints to evaluate the HO_X pool at the
577 site where both anthropogenic and biogenic influences become important factors in

578 determining oxidation capacity. Although the site is in the vicinity of a megacity with 25
579 million people, isoprene accounted for most of the OH loss from observed atmospheric
580 hydrocarbon species during the 6-day focus period in early June 2013 during a regional
581 pollution episode. In addition, observed NO_X levels were substantially lower than
582 observed values in the center of the SMA. These observations indicate that impacts of
583 megacity pollution on suburban BVOC photochemistry can be observed at the TRF.
584 Four different model scenarios are employed to investigate the radical (OH, HO_2,
585 and RO_2) distributions using the UWCM box-model. The observed trace gas data were
586 constrained and the photochemical mechanisms (MCM 3.2) of seven VOC species with
587 high levels at the TRF were integrated. The uncertainty in isoprene peroxy radical
588 chemistry results in a wider range of OH, HO_2, and RO_2 distributions. Unconstrained
589 HONO sources also cause a quite high level of underestimation in a radical pool
590 ($OH+HO_2+RO_2$). OH simulation from the different model scenarios indicates much
591 larger discrepancies (up to three times) than simulations for HO_2 and RO_2 (up to twofold).
592 OH is simulated in higher levels with the consideration of an additional OH recycling
593 channel from fast HPALD formation chemistry Peeters and Muller (2010). On the other
594 hand, the RO_2 simulations result in lower levels as HPALD formation depletes the RO_2
595 pool, which mostly composed by isoprene peroxy radicals. These results suggest that
596 direct HO_2 and RO_2 observations can provide pivotal information about radical recycling
597 and isoprene peroxy radical chemistry (Kim et al., 2013c;Wolfe et al., 2013). More
598 studies on characterizing existing techniques to quantify HO_2 (Fuchs et al., 2011) and
599 developing new techniques (Horstjann et al., 2013) are needed. In addition, the
600 simulations with recently developed isoprene photo-oxidation chemistry show that

601 radical termination processes (e.g. peroxide formation) get more efficient than radical
602 recycling processes in the afternoon. This may come as a surprise as in general we expect
603 the high NO_X conditions in the suburban regions of a megacity to have effective radical
604 recycling. However, the critical factor determining competing reaction channels of
605 recycling and peroxide formation is NO concentrations. Ratios of NO to NO_2 are not only
606 correlated with NO_2 concentrations and photolysis constants but also anti-correlated with
607 RO_2, HO_2 and ozone concentrations and relevant kinetic constants as shown in (Eq 1).
608 Therefore, a semi-quantitative term such as the high 'NO_X' regime is not a proper term to
609 define radical recycle regimes especially in high radical environments (e.g. HO_2 and RO_2)
610 such as forest environments.

611 These uncertainties in estimating the radical pool size and distribution directly
612 affect our ability for constraining photochemical ozone and OVOC production. The non-
613 linear response of ozone production to NO_X and VOC abundances are determined by OH,
614 HO_2, RO_2 and NO_2 concentrations. Regardless of which model calculation scenario we
615 adapt, the TRF photochemical state appears to be a NO_X limited ozone production regime,
616 except for the morning when the VOC limited regime is observed. A noticeable range of
617 NO_X sensitivity was calculated from the four different model scenarios, especially in the
618 afternoon. These analysis results, therefore, suggest that an accurate scientific
619 understanding of isoprene-OH interactions should form the basis for an effective policy
620 implementation to reduce photochemical pollution in the suburbs of Seoul and similar
621 East Asian megacities. In addition, OVOC production is predicted to significantly vary
622 depending on the model simulation scenarios. The fate of these OVOCs is uncertain and
623 can include deposition, photolysis, or condensation. Our limited understanding of

OVOCs contributes substantially to the overall uncertainty in radical photochemistry and should be addressed by studies that quantify the processes controlling OVOC production and loss.

Acknowledgements

This research is financially supported by the National Institute of Environmental Research of South Korea. The authors appreciate logistical support from the research and supporting staff at Taehwa Research Forest operated by Seoul National University.

References

Apel, E. C., Riemer, D. D., Hills, A., Baugh, W., Orlando, J., Faloona, I., Tan, D., Brune, W., Lamb, B., Westberg, H., Carroll, M. A., Thornberry, T., and Geron, C. D.: Measurement and interpretation of isoprene fluxes and isoprene, methacrolein, and methyl vinyl ketone mixing ratios at the PROPHET site during the 1998 Intensive, J Geophys Res-Atmos, 107, Artn 4034
Doi 10.1029/2000jd000225, 2002.

Archibald, A. T., Cooke, M. C., Utembe, S. R., Shallcross, D. E., Derwent, R. G., and Jenkin, M. E.: Impacts of mechanistic changes on HOx formation and recycling in the oxidation of isoprene, Atmos Chem Phys, 10, 8097-8118, Doi 10.5194/Acp-10-8097-2010, 2010a.

Archibald, A. T., Jenkin, M. E., and Shallcross, D. E.: An isoprene mechanism intercomparison, Atmos Environ, 44, 5356-5364, Doi 10.1016/J.Atmosenv.2009.09.016, 2010b.

Arneth, A., Schurgers, G., Lathiere, J., Duhl, T., Beerling, D. J., Hewitt, C. N., Martin, M., and Guenther, A.: Global terrestrial isoprene emission models: sensitivity to variability in climate and vegetation, Atmos Chem Phys, 11, 8037-8052, Doi 10.5194/Acp-11-8037-2011, 2011.

Bao, H., Shrestha, K. L., Kondo, A., Kaga, A., and Inoue, Y.: Modeling the influence of biogenic volatile organic compound emissions on ozone concentration during summer season in the Kinki region of Japan, Atmos Environ, 44, 421-431, Doi 10.1016/J.Atmosenv.2009.10.021, 2010.

Barket, D. J., Hurst, J. M., Couch, T. L., Colorado, A., Shepson, P. B., Riemer, D. D., Hills, A. J., Apel, E. C., Hafer, R., Lamb, B. K., Westberg, H. H., Farmer, C. T., Stabenau, E. R., and Zika, R. G.: Intercomparison of automated methodologies for determination of ambient isoprene during the PROPHET 1998 summer campaign, J Geophys Res-Atmos, 106, 24301-24313, Doi 10.1029/2000jd900562, 2001.

661 Blake, R. S., Monks, P. S., and Ellis, A. M.: Proton-Transfer Reaction Mass
662 Spectrometry, Chem Rev, 109, 861-896, 2009.
663 Bryan, A. M., Bertman, S. B., Carroll, M. A., Dusanter, S., Edwards, G. D., Forkel, R.,
664 Griffith, S., Guenther, A. B., Hansen, R. F., Helmig, D., Jobson, B. T., Keutsch, F.
665 N., Lefer, B. L., Pressley, S. N., Shepson, P. B., Stevens, P. S., and Steiner, A. L.:
666 In-canopy gas-phase chemistry during CABINEX 2009: sensitivity of a 1-D canopy
667 model to vertical mixing and isoprene chemistry, Atmos Chem Phys, 12, 8829-
668 8849, Doi 10.5194/Acp-12-8829-2012, 2012.
669 Chameides, W. L., Lindsay, R. W., Richardson, J., and Kiang, C. S.: The Role of
670 Biogenic Hydrocarbons in Urban Photochemical Smog - Atlanta as a Case-Study,
671 Science, 241, 1473-1475, 1988.
672 Chang, C. C., Wang, J. L., Leung, S.-C. C., Chang, C. Y., Lee, P.-J., Chew, C., Liao, W.-
673 N., and Ou-Yang, C.-F.: Seosonal characteristics of biogenic and anthropogenic
674 isoprene in tropical-subtropical urban environments, Atmos Environ, 99, 298-308,
675 2014.
676 Cheng, H. R., Guo, H., Saunders, S. M., Lam, S. H. M., Jiang, F., Wang, X. M., Simpson,
677 I. J., Blake, D. R., Louie, P. K. K., and Wang, T. J.: Assessing photochemical ozone
678 formation in the Pearl River Delta with a photochemical trajectory model, Atmos
679 Environ, 44, 4199-4208, Doi 10.1016/J.Atmosenv.2010.07.019, 2010.
680 Crounse, J. D., Paulot, F., Kjaergaard, H. G., and Wennberg, P. O.: Peroxy radical
681 isomerization in the oxidation of isoprene, Phys Chem Chem Phys, 13, 13607-
682 13613, Doi 10.1039/C1cp21330j, 2011.
683 de Gouw, J., and Warneke, C.: Measurements of volatile organic compounds in the earths
684 atmosphere using proton-transfer-reaction mass spectrometry, Mass Spectrom Rev,
685 26, 223-257, 2007.
686 Di Carlo, P., Brune, W. H., Martinez, M., Harder, H., Lesher, R., Ren, X. R., Thornberry,
687 T., Carroll, M. A., Young, V., Shepson, P. B., Riemer, D., Apel, E., and Campbell,
688 C.: Missing OH reactivity in a forest: Evidence for unknown reactive biogenic
689 VOCs, Science, 304, 722-725, Doi 10.1126/Science.1094392, 2004.
690 Dreyfus, G. B., Schade, G. W., and Goldstein, A. H.: Observational constraints on the
691 contribution of isoprene oxidation to ozone production on the western slope of the
692 Sierra Nevada, California, J Geophys Res-Atmos, 107, Artn 4365
693 Doi 10.1029/2001jd001490, 2002.
694 Edwards, P. M., Evans, M. J., Furneaux, K. L., Hopkins, J., Ingham, T., Jones, C., Lee, J.
695 D., Lewis, A. C., Moller, S. J., Stone, D., Whalley, L. K., and Heard, D. E.: OH
696 reactivity in a South East Asian tropical rainforest during the Oxidant and Particle
697 Photochemical Processes (OP3) project, Atmos Chem Phys, 13, 9497-9514, Doi
698 10.5194/Acp-13-9497-2013, 2013.
699 Fuchs, H., Bohn, B., Hofzumahaus, A., Holland, F., Lu, K. D., Nehr, S., Rohrer, F., and
700 Wahner, A.: Detection of HO2 by laser-induced fluorescence: calibration and
701 interferences from RO2 radicals, Atmos Meas Tech, 4, 1209-1225, Doi
702 10.5194/Amt-4-1209-2011, 2011.
703 Fuchs, H., Hofzumahaus, A., Rohrer, F., Bohn, B., Brauers, T., Dorn, H. P., Haseler, R.,
704 Holland, F., Kaminski, M., Li, X., Lu, K., Nehr, S., Tillmann, R., Wegener, R., and
705 Wahner, A.: Experimental evidence for efficient hydroxyl radical regeneration in
706 isoprene oxidation, Nat Geosci, 6, 1023-1026, Doi 10.1038/Ngeo1964, 2013.

Ge, B. Z., Sun, Y. L., Liu, Y., Dong, H. B., Ji, D. S., Jiang, Q., Li, J., and Wang, Z. F.: Nitrogen dioxide measurement by cavity attenuated phase shift spectroscopy (CAPS) and implications in ozone production efficiency and nitrate formation in Beijing, China, J Geophys Res-Atmos, 118, 9499-9509, Doi 10.1002/Jgrd.50757, 2013.

Guenther, A.: Biological and chemical diversity of biogenic volatile organic emissions into the atmosphere, Atmospheric Sciences, 2013, ArticleID 786290, 2013.

Hao, N., Zhou, B., Chen, D., and Chen, L. M.: Observations of nitrous acid and its relative humidity dependence in Shanghai, J Environ Sci-China, 18, 910-915, Doi 10.1016/S1001-0742(06)60013-2, 2006.

Hofzumahaus, A., Rohrer, F., Lu, K. D., Bohn, B., Brauers, T., Chang, C. C., Fuchs, H., Holland, F., Kita, K., Kondo, Y., Li, X., Lou, S. R., Shao, M., Zeng, L. M., Wahner, A., and Zhang, Y. H.: Amplified Trace Gas Removal in the Troposphere, Science, 324, 1702-1704, 10.1126/science.1164566, 2009.

Horstjann, M., Andres Hernandez, M. D., Nenakhov, V., Chrobry, A., and Burrows, J. P.: Peroxy radical detection for airborne atmospheric measurements using cavity ehnaced absorption spectroscopy of NO2, Atmospheric Measurement Techniques Discussion, 6, 9655-9688, 2013.

Huang, M., Bowman, K. W., Carmichael, G. R., Pierce, R. B., Worden, H. M., Luo, M., Cooper, O. R., Pollack, I. B., Ryerson, T. B., and Brown, S. S.: Impact of Southern California anthropogenic emissions on ozone pollution in the mountain states: Model analysis and observational evidence from space, J Geophys Res-Atmos, 118, 12784-12803, Doi 10.1002/2013jd020205, 2013.

Kanaya, Y., Pochanart, P., Liu, Y., Li, J., Tanimoto, H., Kato, S., Suthawaree, J., Inomata, S., Taketani, F., Okuzawa, K., Kawamura, K., Akimoto, H., and Wang, Z. F.: Rates and regimes of photochemical ozone production over Central East China in June 2006: a box model analysis using comprehensive measurements of ozone precursors, Atmos Chem Phys, 9, 7711-7723, 2009.

Karl, T., Harley, P., Emmons, L., Thornton, B., Guenther, A., Basu, C., Turnipseed, A., and Jardine, K.: Efficient Atmospheric Cleansing of Oxidized Organic Trace Gases by Vegetation, Science, 330, 816-819, Doi 10.1126/Science.1192534, 2010.

Kim, K. H., Ho, D. X., Park, C. G., Ma, C. J., Pandey, S. K., Lee, S. C., Jeong, H. J., and Lee, S. H.: Volatile Organic Compounds in Ambient Air at Four Residential Locations in Seoul, Korea, Environ Eng Sci, 29, 875-889, Doi 10.1089/Ees.2011.0280, 2012.

Kim, S., Karl, T., Guenther, A., Tyndall, G., Orlando, J., Harley, P., Rasmussen, R., and Apel, E.: Emissions and ambient distributions of Biogenic Volatile Organic Compounds (BVOC) in a ponderosa pine ecosystem: interpretation of PTR-MS mass spectra, Atmos Chem Phys, 10, 1759-1771, 2010.

Kim, S., Guenther, A., Karl, T., and Greenberg, J.: Contributions of primary and secondary biogenic VOC tototal OH reactivity during the CABINEX (Community Atmosphere-Biosphere INteractions Experiments)-09 field campaign, Atmos Chem Phys, 11, 8613-8623, 2011.

Kim, S., Guenther, A., and Apel, E.: Quantitative and qualitative sensing techniques for biogenic volatile organic compounds and their oxidation products, Environ Sci-Proc Imp, 15, 1301-1314, Doi 10.1039/C3em00040k, 2013a.

753 Kim, S., Lee, M., Kim, S., Choi, S., Seok, S., and Kim, S.: Photochemical characteristics
754 of high and low ozone episodes observed in the Taehwa Forest observatory (TFO)
755 in June 2011 near Seoul South Korea, Asia-Pacific Journal of Atmospheric
756 Sciences, 49, 325-331, Doi 10.1007/S13143-013-0031-0, 2013b.
757 Kim, S., Wolfe, G. M., Mauldin, L., Cantrell, C., Guenther, A., Karl, T., Turnipseed, A.,
758 Greenberg, J., Hall, S. R., Ullmann, K., Apel, E., Hornbrook, R., Kajii, Y.,
759 Nakashima, Y., Keutsch, F. N., DiGangi, J. P., Henry, S. B., Kaser, L.,
760 Schnitzhofer, R., Graus, M., Hansel, A., Zheng, W., and Flocke, F. F.: Evaluation
761 of HOx sources and cycling using measurement-constrained model calculations in a
762 2-methyl-3-butene-2-ol (MBO) and monoterpene (MT) dominated ecosystem,
763 Atmos Chem Phys, 13, 2031-2044, Doi 10.5194/Acp-13-2031-2013, 2013c.
764 Kim, S., VandenBoer, T. C., Young, C. J., Riedel, T. P., Thornton, J. A., Swarthout, B.,
765 Sive, B., Lerner, B., Gilman, J. B., Warneke, C., Roberts, J. M., Guenther, A.,
766 Wagner, N. L., Dube, W. P., Williams, E., and Brown, S. S.: The primary and
767 recycling sources of OH during the NACHTT-2011 campaign: HONO as an
768 important OH primary source in the wintertime, J Geophys Res-Atmos, 119, 6886-
769 6896, Doi 10.1002/2013jd019784, 2014.
770 Kim, S. Y., Jiang, X. Y., Lee, M., Turnipseed, A., Guenther, A., Kim, J. C., Lee, S. J.,
771 and Kim, S.: Impact of biogenic volatile organic compounds on ozone production at
772 the Taehwa Research Forest near Seoul, South Korea, Atmos Environ, 70, 447-453,
773 Doi 10.1016/J.Atmosenv.2012.11.005, 2013d.
774 Kleinman, L. I.: Ozone process insights from field experiments - part II: Observation-
775 based analysis for ozone production, Atmos Environ, 34, 2023-2033, Doi
776 10.1016/S1352-2310(99)00457-4, 2000.
777 Leighton, P. A.: Photochemistry of Air Pollution, Academic, San Diego, CA USA, 1961.
778 Lelieveld, J., Butler, T. M., Crowley, J. N., Dillon, T. J., Fischer, H., Ganzeveld, L.,
779 Harder, H., Lawrence, M. G., Martinez, M., Taraborrelli, D., and Williams, J.:
780 Atmospheric oxidation capacity sustained by a tropical forest, Nature, 452, 737-
781 740, 2008.
782 Levy, H.: Normal Atmosphere - Large Radical and Formaldehyde Concentrations
783 Predicted, Science, 173, 141-143, 1971.
784 Li, X., Brauers, T., Haseler, R., Bohn, B., Fuchs, H., Hofzumahaus, A., Holland, F., Lou,
785 S., Lu, K. D., Rohrer, F., Hu, M., Zeng, L. M., Zhang, Y. H., Garland, R. M., Su,
786 H., Nowak, A., Wiedensohler, A., Takegawa, N., Shao, M., and Wahner, A.:
787 Exploring the atmospheric chemistry of nitrous acid (HONO) at a rural site in
788 Southern China, Atmos Chem Phys, 12, 1497-1513, 2012.
789 Li, Y., Lau, A. K. H., Fung, J. C. H., Zheng, J. Y., and Liu, S. C.: Importance of NOx
790 control for peak ozone reduction in the Pearl River Delta region, J Geophys Res-
791 Atmos, 118, 9428-9443, Doi 10.1002/Jgrd.50659, 2013.
792 Lim, Y. J., Armendariz, A., Son, Y. S., and Kim, J. C.: Seasonal variations of isoprene
793 emissions from five oak tree species in East Asia, Atmos Environ, 45, 2202-2210,
794 Doi 10.1016/J.Atmosenv.2011.01.066, 2011.
795 Liu, Y. J., Herdlinger-Blatt, I., McKinney, K. A., and Martin, S. T.: Production of methyl
796 vinyl ketone and methacrolein via the hydroperoxyl pathway of isoprene oxidation,
797 Atmospheric Chemistry and Physics, 13, 5715-5730, Doi 10.5194/Acp-13-5715-
798 2013, 2013.

Lou, S., Holland, F., Rohrer, F., Lu, K., Bohn, B., Brauers, T., Chang, C. C., Fuchs, H., Haseler, R., Kita, K., Kondo, Y., Li, X., Shao, M., Zeng, L., Wahner, A., Zhang, Y., Wang, W., and Hofzumahaus, A.: Atmospheric OH reactivities in the Pearl River Delta - China in summer 2006: measurement and model results, Atmos Chem Phys, 10, 11243-11260, 2010.

Lu, K. D., Rohrer, F., Holland, F., Fuchs, H., Bohn, B., Brauers, T., Chang, C. C., Haseler, R., Hu, M., Kita, K., Kondo, Y., Li, X., Lou, S. R., Nehr, S., Shao, M., Zeng, L. M., Wahner, A., Zhang, Y. H., and Hofzumahaus, A.: Observation and modelling of OH and HO2 concentrations in the Pearl River Delta 2006: a missing OH source in a VOC rich atmosphere, Atmos Chem Phys, 12, 1541-1569, Doi 10.5194/Acp-12-1541-2012, 2012.

Ma, J. Z., Wang, W., Chen, Y., Liu, H. J., Yan, P., Ding, G. A., Wang, M. L., Sun, J., and Lelieveld, J.: The IPAC-NC field campaign: a pollution and oxidization pool in the lower atmosphere over Huabei, China, Atmos Chem Phys, 12, 3883-3908, Doi 10.5194/Acp-12-3883-2012, 2012.

Mannschreck, K., Gilge, S., Plass-Duelmer, C., Fricke, W., and Berresheim, H.: Assessment of the applicability of NO-NO2-O-3 photostationary state to long-term measurements at the Hohenpeissenberg GAW Station, Germany, Atmos Chem Phys, 4, 1265-1277, 2004.

Mao, J., Ren, X., Zhang, L., Van Duin, D. M., Cohen, R. C., Park, J. H., Goldstein, A. H., Paulot, F., Beaver, M. R., Crounse, J. D., Wennberg, P. O., DiGangi, J. P., Henry, S. B., Keutsch, F. N., Park, C., Schade, G. W., Wolfe, G. M., Thornton, J. A., and Brune, W. H.: Insights into hydroxyl measurements and atmospheric oxidation in a California forest, Atmos Chem Phys, 12, 8009-8020, Doi 10.5194/Acp-12-8009-2012, 2012.

Mao, J. Q., Ren, X. R., Chen, S. A., Brune, W. H., Chen, Z., Martinez, M., Harder, H., Lefer, B., Rappengluck, B., Flynn, J., and Leuchner, M.: Atmospheric oxidation capacity in the summer of Houston 2006: Comparison with summer measurements in other metropolitan studies, Atmos Environ, 44, 4107-4115, Doi 10.1016/J.Atmosenv.2009.01.013, 2010.

Na, K., and Kim, Y. P.: Seasonal characteristics of ambient volatile organic compounds in Seoul, Korea, Atmos Environ, 35, 2603-2614, Doi 10.1016/S1352-2310(00)00464-7, 2001.

Nakashima, Y., Kato, S., Greenberg, J., Harley, P., Karl, T., Turnipseed, A., Apel, E., Guenther, A., Smith, J., and Kajii, Y.: Total OH reactivity measurements in ambient air in a southern Rocky mountain ponderosa pine forest during BEACHON-SRM08 summer campaign, Atmos Environ, 85, 1-8, Doi 10.1016/J.Atmosenv.2013.11.042, 2014.

NIER: Annual Report for Atmospheric Environment, National Insititute of Environmetal Rsearch, 2010.

Nolscher, A. C., Williams, J., Sinha, V., Custer, T., Song, W., Johnson, A. M., Axinte, R., Bozem, H., Fischer, H., Pouvesle, N., Phillips, G., Crowley, J. N., Rantala, P., Rinne, J., Kulmala, M., Gonzales, D., Valverde-Canossa, J., Vogel, A., Hoffmann, T., Ouwersloot, H. G., de Arellano, J. V. G., and Lelieveld, J.: Summertime total OH reactivity measurements from boreal forest during HUMPPA-COPEC 2010, Atmos Chem Phys, 12, 8257-8270, Doi 10.5194/Acp-12-8257-2012, 2012.

Oswald, R., Behrendt, T., Ermel, M., Wu, D., Su, H., Cheng, Y., Breuninger, C., Moravek, A., Mougin, E., Delon, C., Loubet, B., Pommerening-Roser, A., Sorgel, M., Poschl, U., Hoffmann, T., Andreae, M. O., Meixner, F. X., and Trebs, I.: HONO Emissions from Soil Bacteria as a Major Source of Atmospheric Reactive Nitrogen, Science, 341, 1233-1235, Doi 10.1126/Science.1242266, 2013.

Paulot, F., Crounse, J. D., Kjaergaard, H. G., Kroll, J. H., Seinfeld, J. H., and Wennberg, P. O.: Isoprene photooxidation: new insights into the production of acids and organic nitrates, Atmos Chem Phys, 9, 1479-1501, 2009.

Paulson, S. E., and Seinfeld, J. H.: Development and evaluation of a photooxidation mechanism for isoprene, Journal of Geophysical Research, 97, 20703-20715, 1992.

Peeters, J., and Muller, J. F.: HOx radical regeneration in isoprene oxidation via peroxy radical isomerisations. II: experimental evidence and global impact, Phys Chem Chem Phys, 12, 14227-14235, Doi 10.1039/C0cp00811g, 2010.

Pollack, I. B., Ryerson, T. B., Trainer, M., Neuman, J. A., Roberts, J. M., and Parrish, D. D.: Trends in ozone, its precursors, and related secondary oxidation products in Los Angeles, California: A synthesis of measurements from 1960 to 2010, J Geophys Res-Atmos, 118, 5893-5911, Doi 10.1002/Jgrd.50472, 2013.

Ran, L., Zhao, C. S., Xu, W. Y., Lu, X. Q., Han, M., Lin, W. L., Yan, P., Xu, X. B., Deng, Z. Z., Ma, N., Liu, P. F., Yu, J., Liang, W. D., and Chen, L. L.: VOC reactivity and its effect on ozone production during the HaChi summer campaign, Atmos Chem Phys, 11, 4657-4667, Doi 10.5194/Acp-11-4657-2011, 2011.

Ren, X., Sanders, J. E., Rajendran, A., Weber, R. J., Goldstein, A. H., Pusede, S. E., Browne, E. C., Min, K. E., and Cohen, R. C.: A relaxed eddy accumulation system for measuring vertical fluxes of nitrous acid, Atmos Meas Tech, 4, 2093-2103, Doi 10.5194/Amt-4-2093-2011, 2011.

Ryerson, T. B., Andrews, A. E., Angevine, W. M., Bates, T. S., Brock, C. A., Cairns, B., Cohen, R. C., Cooper, O. R., de Gouw, J. A., Fehsenfeld, F. C., Ferrare, R. A., Fischer, M. L., Flagan, R. C., Goldstein, A. H., Hair, J. W., Hardesty, R. M., Hostetler, C. A., Jimenez, J. L., Langford, A. O., McCauley, E., McKeen, S. A., Molina, L. T., Nenes, A., Oltmans, S. J., Parrish, D. D., Pederson, J. R., Pierce, R. B., Prather, K., Quinn, P. K., Seinfeld, J. H., Senff, C. J., Sorooshian, A., Stutz, J., Surratt, J. D., Trainer, M., Volkamer, R., Williams, E. J., and Wofsy, S. C.: The 2010 California Research at the Nexus of Air Quality and Climate Change (CalNex) field study, J Geophys Res-Atmos, 118, 5830-5866, Doi 10.1002/Jgrd.50331, 2013.

Ryu, Y. H., Baik, J. J., Kwak, K. H., Kim, S., and Moon, N.: Impacts of urban land-surface forcing on ozone air quality in the Seoul metropolitan area, Atmos Chem Phys, 13, 2177-2194, Doi 10.5194/Acp-13-2177-2013, 2013.

Sartelet, K. N., Couvidat, F., Seigneur, C., and Roustan, Y.: Impact of biogenic emissions on air quality over Europe and North America, Atmos Environ, 53, 131-141, Doi 10.1016/J.Atmosenv.2011.10.046, 2012.

Shao, M., Lu, S. H., Liu, Y., Xie, X., Chang, C. C., Huang, S., and Chen, Z. M.: Volatile organic compounds measured in summer in Beijing and their role in ground-level ozone formation, J Geophys Res-Atmos, 114, Artn D00g06
Doi 10.1029/2008jd010863, 2009a.

Shao, M., Zhang, Y. H., Zeng, L. M., Tang, X. Y., Zhang, J., Zhong, L. J., and Wang, B. G.: Ground-level ozone in the Pearl River Delta and the roles of VOC and NO(x) in its production, J Environ Manage, 90, 512-518, Doi 10.1016/J.Jenvman.2007.12.008, 2009b.

Sillman, S., and He, D.: Some theoretical results concerning O3-NOx-VOC chemistry and NOx-VOC indicators, Journal of Geophysical Research, 107, 4659,doi:4610.1029:2001JD001123, 2002.

Sinha, V., Williams, J., Lelieveld, J., Ruuskanen, T. M., Kajos, M. K., Patokoski, J., Hellen, H., Hakola, H., Mogensen, D., Boy, M., Rinne, J., and Kulmala, M.: OH Reactivity Measurements within a Boreal Forest: Evidence for Unknown Reactive Emissions, Environ Sci Technol, 44, 6614-6620, Doi 10.1021/Es101780b, 2010.

Song, C. H., Park, M. E., Lee, E. J., Lee, J. H., Lee, B. K., Lee, D. S., Kim, J., Han, J. S., Moon, K. J., and Kondo, Y.: Possible particulate nitrite formation and its atmospheric implications inferred from the observations in Seoul, Korea, Atmos Environ, 43, 2168-2173, Doi 10.1016/J.Atmosenv.2009.01.018, 2009.

Spaulding, R. S., Schade, G. W., Goldstein, A. H., and Charles, M. J.: Characterization of secondary atmospheric photooxidation products: Evidence for biogenic and anthropogenic sources, J Geophys Res-Atmos, 108, Artn 4247
Doi 10.1029/2002jd002478, 2003.

Steinbacher, M., Zellweger, C., Schwarzenbach, B., Bugmann, S., Buchmann, B., Ordonez, C., Prevot, A. S. H., and Hueglin, C.: Nitrogen oxide measurements at rural sites in Switzerland: Bias of conventional measurement techniques, J Geophys Res-Atmos, 112, Artn D11307
Doi 10.1029/2006jd007971, 2007.

Tie, X., Geng, F., Guenther, A., Cao, J., Greenberg, J., Zhang, R., Apel, E., Li, G., Weinheimer, A., Chen, J., and Cai, C.: Megacity impacts on regional ozone formation: observations and WRF-Chem modeling for the MIRAGE-Shanghai field campaign, Atmos Chem Phys, 13, 5655-5669, Doi 10.5194/Acp-13-5655-2013, 2013.

Tonnesen, G. S., and Dennis, R. L.: Analysis of radical propagation efficiency to assess ozone sensitivity to hydrocarbons and NOx 1. Local indicators of instantaneous odd oxygen production sensitivity, J Geophys Res-Atmos, 105, 9213-9225, Doi 10.1029/1999jd900371, 2000a.

Tonnesen, G. S., and Dennis, R. L.: Analysis of radical propagation efficiency to assess ozone sensitivity to hydrocarbons and NOx 2. Long-lived species as indicators of ozone concentration sensitivity, J Geophys Res-Atmos, 105, 9227-9241, Doi 10.1029/1999jd900372, 2000b.

Trainer, M., Williams, E., Parrish, D. D., Buhr, M. P., Allwine, E. J., Westberg, H., Fehsenfeld, F. C., and Liu, S. C.: Models and observations of the impact of natural hydrocarbons on rural ozone, Nature, 329, 705 - 707, 1987.

Tseng, K. H., Wang, J. L., Cheng, M. T., and Tsuang, B. J.: Assessing the Relationship between Air Mass Age and Summer Ozone Episodes Based on Photochemical Indices, Aerosol Air Qual Res, 9, 149-171, 2009.

VandenBoer, T., Murphy, J. G., Roberts, J. M., Middlebrook, A. M., Brock, C., Lerner, B. M., Wolfe, D. E., Williams, E., Brown, S. S., Warneke, C., De Gouw, J., Wagner, N. L., Young, C. C., Dube, W. P., Bahreini, R., Riedel, T., Thornton, J. A.,

936 Ozturk, F., Keene, W., Maben, J. R., Pszenny, A., Kim, S., Grossberg, N., and
937 Lefer, B.: Understanding the role of the ground surface in HONO vertical structure:
938 High resolution vertical profiles during NACHTT-11, submitted, 2013.
939 Villena, G., Bejan, I., Kurtenbach, R., Wiesen, P., and Kleffmann, J.: Interferences of
940 commercial NO2 instruments in the urban atmosphere and in a smog chamber,
941 Atmos Meas Tech, 5, 149-159, Doi 10.5194/Amt-5-149-2012, 2012.
942 Wolfe, G. M., and Thornton, J. A.: The chemistry of atmosphere-forest exchange (CAFE)
943 model - PART1: Model description and characterization, Atmos Chem Phys, 11,
944 77-101, 2011.
945 Wolfe, G. M., Crounse, J. D., Parrish, J. D., St Clair, J. M., Beaver, M. R., Paulot, F.,
946 Yoon, T. P., Wennberg, P. O., and Keutsch, F. N.: Photolysis, OH reactivity and
947 ozone reactivity of a proxy for isoprene-derived hydroperoxyenals (HPALDs), Phys
948 Chem Chem Phys, 14, 7276-7286, 2012.
949 Wolfe, G. M., Cantrell, C., Kim, S., Mauldin, R., Karl, T., Harley, P., Turnipseed, A.,
950 Zheng, W., Flocke, F., Apel, E., Hornbrook, R. S., Hall, S., Ullmann, K., Henry, S.
951 B., Digangi, J., Boyle, E. S., Kaser, L., Schnitzhofer, R., Hansel, A., Graus, M.,
952 Nakashima, Y., Kajii, Y., Guenther, A., and Keutsch, F.: Missing peroxy radical
953 sources within a rural forest canopy, Atmospheric Chemistry and Physics
954 Discussion, 13, 31713-31759, 2013.
955 Wong, K. W., Tsai, C., Lefer, B., Haman, C., Grossberg, N., Brune, W. H., Ren, X.,
956 Luke, W., and Stutz, J.: Daytime HONO vertical gradients during SHARP 2009 in
957 Houston, TX, Atmos Chem Phys, 12, 635-652, Doi 10.5194/Acp-12-635-2012,
958 2012.
959 Xing, J., Wang, S. X., Jang, C., Zhu, Y., and Hao, J. M.: Nonlinear response of ozone to
960 precursor emission changes in China: a modeling study using response surface
961 methodology, Atmos Chem Phys, 11, 5027-5044, Doi 10.5194/Acp-11-5027-2011,
962 2011.
963 Yoshino, A., Nakashima, Y., Miyazaki, K., Kato, S., Suthawaree, J., Shimo, N.,
964 Matsunaga, S., Chatani, S., Apel, E., Greenberg, J., Guenther, A., Ueno, H., Sasaki,
965 H., Hoshi, J., Yokota, H., Ishii, K., and Kajii, Y.: Air quality diagnosis from
966 comprehensive observations of total OH reactivity and reactive trace species in
967 urban central Tokyo, Atmos Environ, 49, 51-59, Doi
968 10.1016/J.Atmosenv.2011.12.029, 2012.
969 Yuan, B., Warneke, C., Shao, M., and de Gouw, J. A.: Interpretation of volatile organic
970 compound measurements by proton-transfer-reaction mass spectrometry over the
971 deepwater horizon oil spill, International Journal of Mass Spectrometry, 358, 43-48,
972 Doi 10.1016/J.Ijms.2013.11.006, 2014.
973 Zhang, Y., Hu, X. M., Leung, L. R., and Gustafson, W. I.: Impacts of regional climate
974 change on biogenic emissions and air quality, J Geophys Res-Atmos, 113, Artn
975 D18310
976 Doi 10.1029/2008jd009965, 2008a.
977 Zhang, Y. H., Su, H., Zhong, L. J., Cheng, Y. F., Zeng, L. M., Wang, X. S., Xiang, Y. R.,
978 Wang, J. L., Gao, D. F., Shao, M., Fan, S. J., and Liu, S. C.: Regional ozone
979 pollution and observation-based approach for analyzing ozone-precursor
980 relationship during the PRIDE-PRD2004 campaign, Atmos Environ, 42, 6203-
981 6218, Doi 10.1016/J.Atmosenv.2008.05.002, 2008b.

Zhao, J., and Zhang, R. Y.: Proton transfer reaction rate constants between hydronium ion (H3O(+)) and volatile organic compounds, Atmos Environ, 38, 2177-2185, 2004.

Zhou, X. L., Zhang, N., TerAvest, M., Tang, D., Hou, J., Bertman, S., Alaghmand, M., Shepson, P. B., Carroll, M. A., Griffith, S., Dusanter, S., and Stevens, P. S.: Nitric acid photolysis on forest canopy surface as a source for tropospheric nitrous acid, Nat Geosci, 4, 440-443, 2011.

990

991 Table 1. Analytical characteristics of trace gas analyzers at TRF

992

Chemical Species	Manufacturer and Model Number	Uncertainty	Lower Limit of Detection
CO	Thermo Scientific 48i TLE	10%	40 ppb
NO_X	Thermo Scientific 42i-TL with a Mo-converter	15%	50 ppt
SO_2	Thermo Scientific 43i-TLE	10%	50 ppt
ozone	Thermo Scientific 49i	5%	< 1 ppb

993
994

Table 2. Terpenoid speciation analysis results from GC-MS a) branch enclosure and b) ambient air samples.

a)

Terpenoids	*Composition(%)	Speciation	*Composition(%)
Isoprene	0.5		
Monoterpenes	92.9	α-pinene	36.7
		camphene	13.1
		β-pinene	12.0
		β-myrcene	27.7
		α-terpinolene	1.9
		d-limonene	8.6
Sesquiterpenes	6.6	β-caryophyllene	53.2
		α-caryophyllene	46.8

b)

Terpeniods	*Composition(%)	Speciation	*Composition(%)
Monoterpenes	98.6	α-pinene	38.8
		β-piene	36.5
		camphene	13.5
		d-limonene	11
Sesquiterpenes	1.4	longifolene	100

*Composition is calculated based on the mixing ratio scale

Table 3. A summary of critical differences in input parameters for four different model simulation scenarios presented in this study. The isoprene chemical scheme is based on Archibald et al. (2010a).

	HPALD chemistry	Observational Constraints
Scenario I	No	$^{-}$All
Scenario II	$^{\#}$Peeters and Muller (2010)	$^{-}$All
Scenario III	$^{+}$Crounse et al. (2011)	$^{-}$All
Scenario IV	No	$^{-}$All but HONO

$^{\#}$k298 = ~ 0.08 for isoprene peroxy radical isomerization rate leading to produce HPALD, $^{+}$k298 = 0.002 for isoprene peroxy radical isomerization rate, $^{-}$All the observed diurnal variations, appeared in Figure 1 are constrained in the model along with ambient pressure and humidity.

Table 4 A summary for radical distributions from the observationally constrained box-model simulation results

	OH		HO_2		RO_2		Constraints
Local Time	8:00-12:00	13:00-16:00	8:00-12:00	13:00-16:00	8:00-12:00	13:00-16:00	
Scenario I	3.85×10^6	3.08×10^6	4.10×10^8	7.02×10^8	3.65×10^8	1.14×10^9	All
Scenario II	3.99×10^6	3.69×10^6	3.99×10^8	7.86×10^8	3.51×10^8	9.62×10^8	All
Scenario III	3.86×10^6	3.13×10^6	4.09×10^8	7.09×10^8	3.64×10^8	1.12×10^9	All
Scenario IV	1.61×10^6	1.61×10^6	1.95×10^8	4.82×10^8	1.75×10^8	7.25×10^8	All but HONO

unit: molecules cm^{-3}

Figure 1. Averaged temporal variations observed trace gases and ambient temperature at TRF (June 1st to June 6th, 2012, KST stands for Korean Standard Time GMT+9). The uncertainty for each observable is listed in the main text.

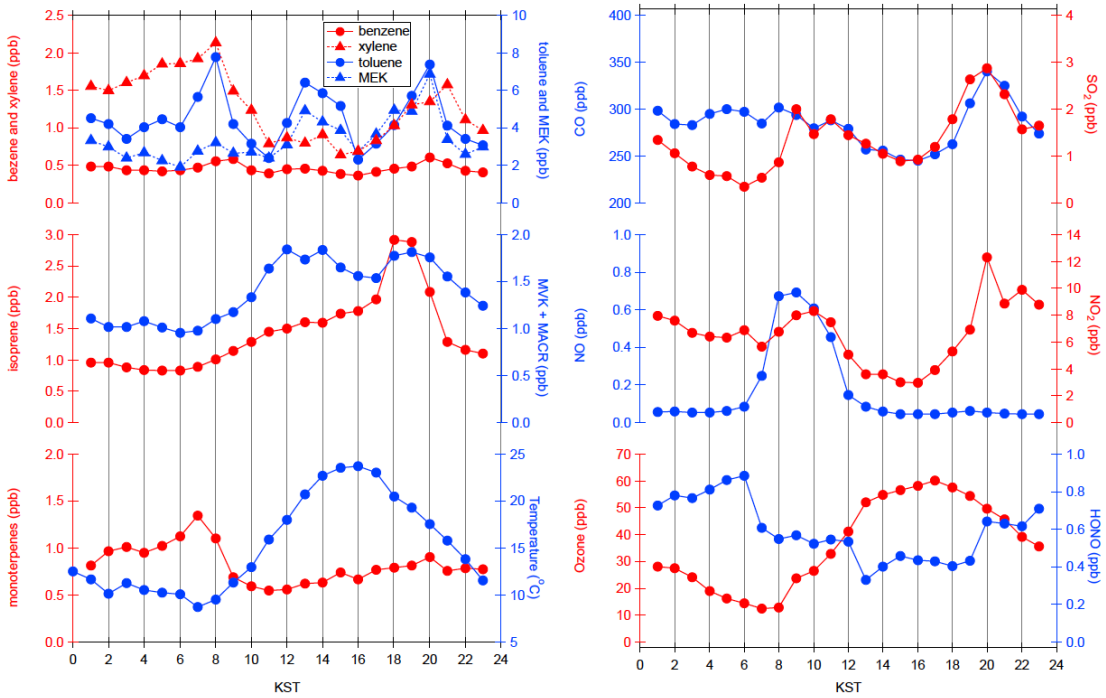

Figure 2. The temporal variations of OH reactivity calculated from the observed dataset at TRF (Figure 1).

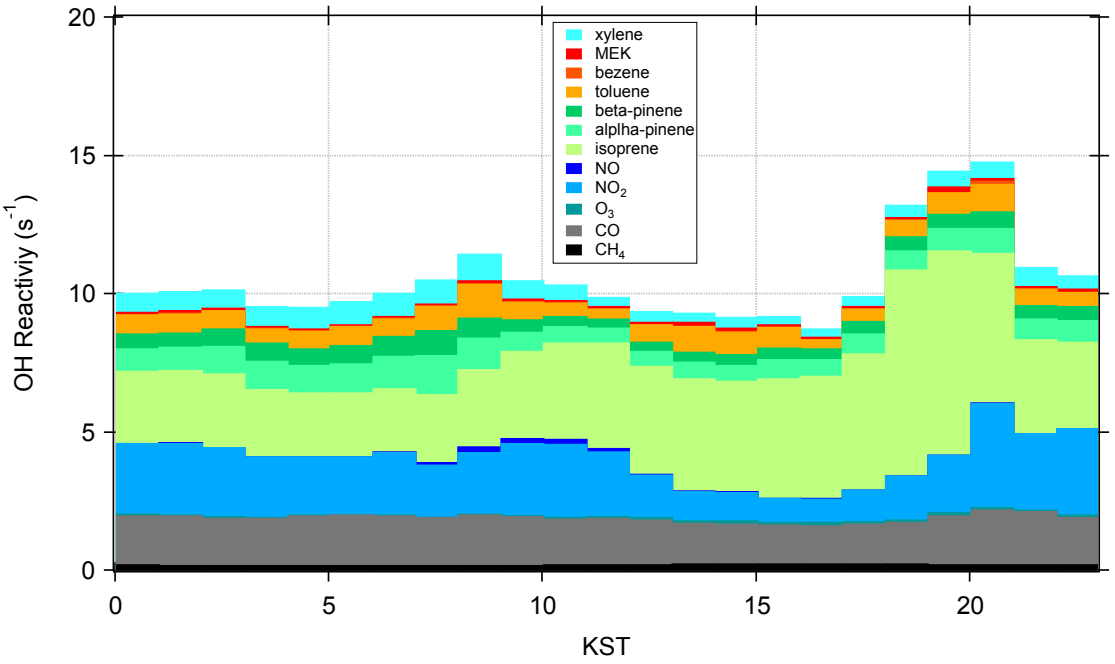

Figure 3. The temporal variations of OH (a), HO_2 (b) , and RO_2 (c) calculated by four different observationally constrained UWCM box model scenarios.

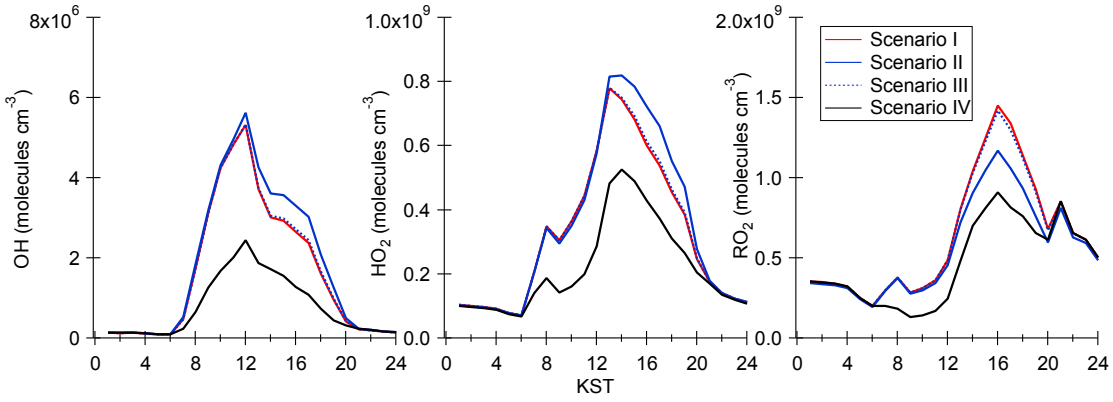

Figure 4 The temporal variations of radical recycling (red) and destruction (blue, black and green) rates calculated using the UWCM box model for different model scenarios

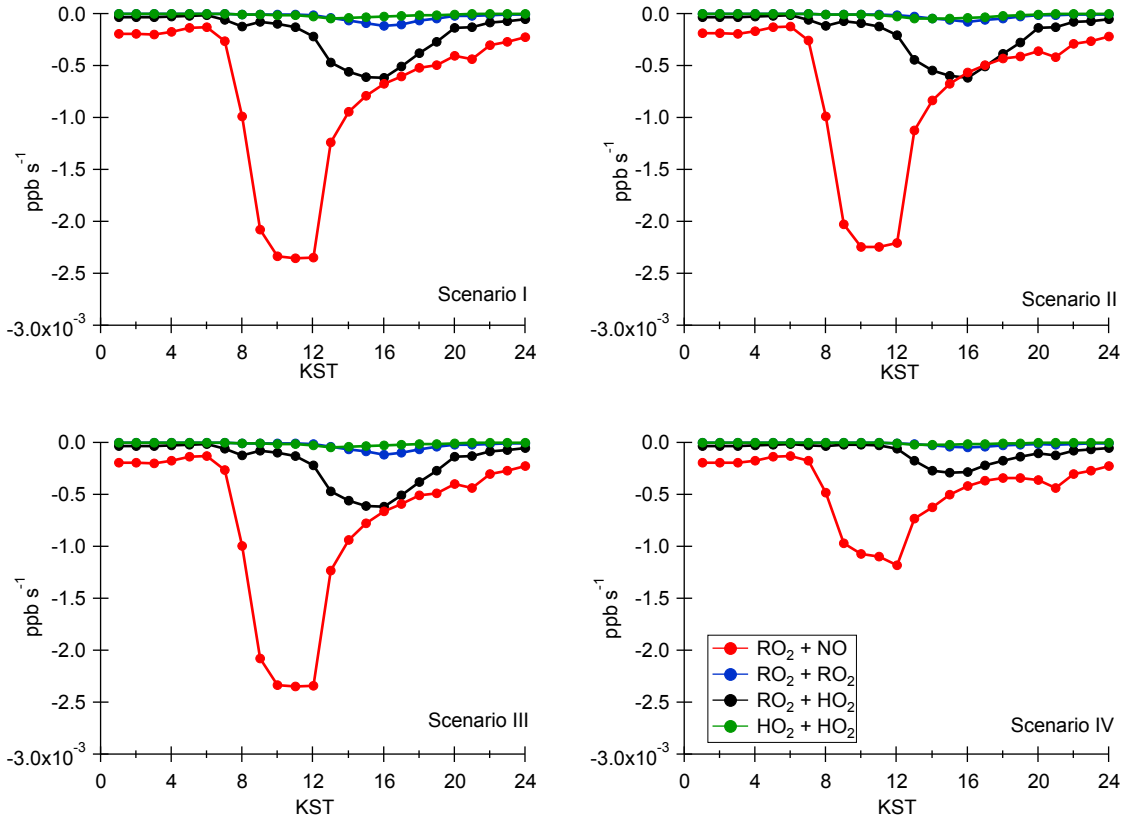

Figure 5. The temporal variations of P_{H2O2}/P_{HNO3} calculated from the UWCM box model from four different model scenarios

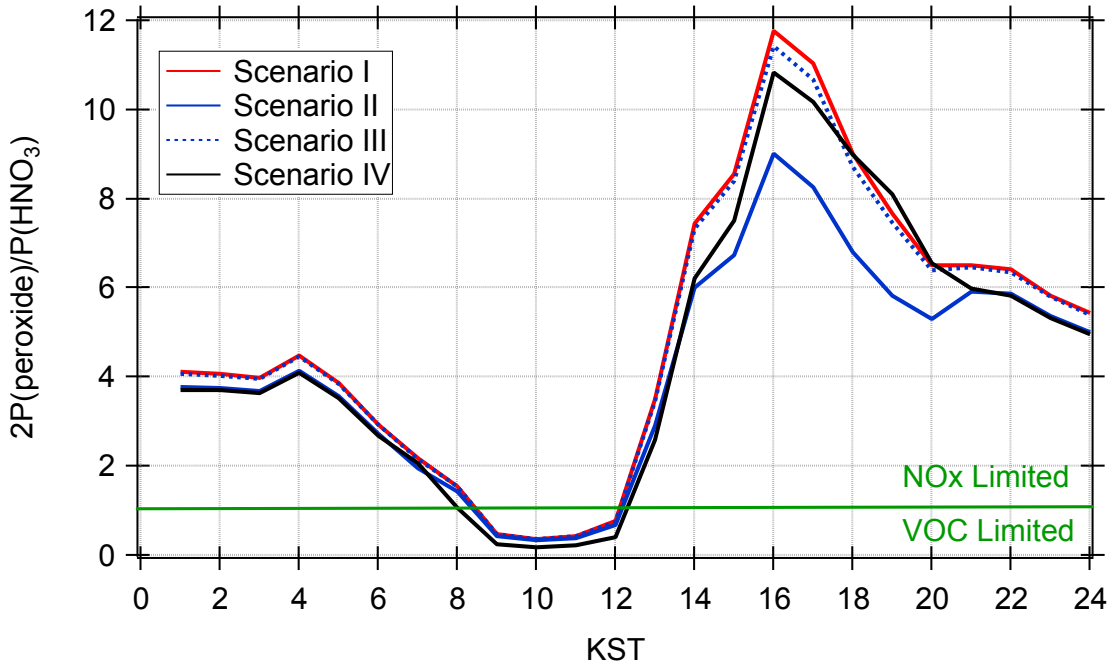

Figure 6. The temporal distributions of UWCM calculated OH reactivity (a) and formaldehyde (b) from different model calculation scenarios